Proc. Estonian Acad. Sci. Phys. Math., 2003, **52**, 3, 308–320

# Effects of growth temperature on the properties of $HfO_2$ films grown by atomic layer deposition

Giovanna Scarel, Claudia Wiemer, Sandro Ferrari, Grazia Tallarida, and Marco Fanciulli

Laboratorio MDM-INFM, Via C. Olivetti 2, 20041 Agrate Brianza (MI), Italy; giovanna.scarel@mi.infm.it

Received 20 January 2003, in revised form 20 March 2003

**Abstract.** A relatively high dielectric constant ($\kappa$ = 20–25), wide band gap and conduction band offset (6.0 eV and 1.5 eV, respectively), and good thermal stability upon contact with silicon indicate hafnium dioxide as one of the most promising candidates to substitute silicon dioxide as dielectric gate in complementary metal-oxide-semiconductor devices. To investigate the properties of thin films suitable for application in microelectronics, $HfO_2$ films were grown by atomic layer deposition. Hafnium tetrachloride ($HfCl_4$) and water ($H_2O$) were used as precursors. Film structural, morphological, and compositional properties were then investigated focusing on their dependence on growth temperature in the range between 150 °C and 350 °C. A modification of the film structure with growth temperature is expected because the density of the reactive OH sites is known to decrease with increasing temperature. The extent and consequences of these modifications were investigated using X-ray diffraction and reflectivity, and atomic force microscopy. Time of flight–secondary ion mass spectrometry was used to study film composition.

**Key words:** atomic layer deposition, $HfO_2$, $ZnO_2$, dielectric oxides.

## 1. INTRODUCTION

Hafnium dioxide is one of the most promising candidates to substitute $SiO_2$ as high dielectric constant ($\kappa$) gate dielectric in complementary metal-oxide-semiconductor (CMOS) devices [1]. The appealing properties of $HfO_2$ are: a high dielectric constant ($\kappa$ = 21, [2]), wide band gap and conduction band offset (6.0 eV and 1.5 eV, respectively, [3,4]), thermodynamical stability upon contact with silicon [5,6]. The properties of thin $HfO_2$, however, depend largely upon many

factors, among them the growth technique, the growth parameters, and the substrate preparation.

In this work we studied films grown by atomic layer deposition (ALD) because this deposition technique is of great interest in microelectronics [1]. Indeed, due to self-limiting reactions, ALD produces uniform, conformal, and easily controllable films [7]. In many cases ALD high-$\kappa$ oxides have shown not to form silicates when grown on silicon [8]. Upon deposition, we studied the effects of one of the growth parameters, the substrate temperature during growth ($T_g$), on the properties of $HfO_2$ films grown on a silicon substrate with native oxide.

The main purpose of this work is to investigate the role of $T_g$ in tuning the structural and compositional properties of $HfO_2$ films grown by ALD. It is expected that $T_g$ affects such properties because of its influence on the type and number of bonds between the superficial silicon atoms and their surroundings [9]. In addition, different values of $T_g$ might induce different chemistry during the growth process. Such phenomena were indeed observed in $ZrO_2$ films, also grown by ALD [10–12] within very similar conditions to the $HfO_2$ films analysed in this work. An indication about $T_g$ inducing modifications also in $HfO_2$ films was found by Cho et al. [13], although those authors studied films grown on HF-treated Si(1 0 0) substrates.

## 2. EXPERIMENTAL PROCEDURE

Hafnium dioxide films were grown by ALD in a flow type F-120 ASM-Microchemistry reactor. Si(1 0 0) *p*-type wafers were used as substrates without removing the native oxide. The precursors were $HfCl_4$ and $H_2O$, carried into the growth chamber by $N_2$ in, respectively, 4 s and 6 s long pulses. The source temperatures were 160 °C for $HfCl_4$ and 18 °C for $H_2O$. Five films were grown at different temperatures ranging from 150 °C to 350 °C (Table 1). For each film, 190 pulse/purge cycles were programmed. During growth, the pressure in the reactor was of the order of $10^{-3}$ bar. No post-deposition treatment was performed on any of the films.

**Table 1.** Growth temperature ($T_g$), thickness ($d$), growth rate ($\gamma$), density ($\delta$), and film surface roughness ($\sigma_{XRR}$) from the fitting of the X-ray reflectivity (XRR) spectra of the films studied in this work. The error on $d$ and $\sigma_{XRR}$ is ± 0.1 nm. The error on $\delta$ is ± 0.001 Å$^{-1}$

| Film | $T_g$, °C | $d$, nm | $\gamma$, nm/cy | $\delta$, Å$^{-1}$ | $\sigma_{XRR}$, nm |
|---|---|---|---|---|---|
| *a* | 150 | 34.1 | 0.18 | 0.051 | 0.6 |
| *b* | 200 | 28.9 | 0.15 | 0.053 | 0.7 |
| *c* | 250 | 21.3 | 0.11 | 0.055 | 1.0 |
| *d* | 300 | 16.0 | 0.08 | 0.058 | 0.6 |
| *e* | 350 | 15.7 | 0.08 | 0.058 | 0.7 |

Grazing incidence X-ray diffraction (GIXRD) and X-ray reflectivity (XRR) measurements were performed using an instrument equipped with a position sensitive detector (INEL CPS 120) and a single point scintillator. The position sensitive detector is capable of collecting data over a 120° range at a time. A multilayer monochromator, placed between the source and the sample, selects the Cu K$\alpha$ radiation. In front of the sample holder a system of variable cross slits allows a proper selection of the beam size. The sample is placed on a four-circle goniometer. The diffraction patterns were collected in grazing incidence geometry at a fixed angle of 0.5° and in a time range of 3 hours. The reflectivity data, instead, were collected with the point detector in a $\Theta$–$2\Theta$ mode. The monochromator and slits configuration defined a resolution of $2 \times 10^{-4}$ Å$^{-1}$. Data were acquired between 0° and 10° with a $2\Theta$ step of 0.02°.

Atomic force microscopy (AFM) measurements were performed using a commercial system properly isolated from vibrations and noise (background noise lower than 0.4 Å-rms), and equipped with a high-resolution scanner. The best results were obtained by operating in the non-contact mode, using high-frequency ($\approx$ 190 kHz) conical silicon probes with typical tip curvature radius of less than 15 nm. The images are square scans of either 1 $\mu$m (films *a* and *b*) or 2.3 $\mu$m (films *c* through *e*) side, with a resolution of 300 points $\times$ 300 lines. Several measurements were taken on each film to ensure reproducibility.

Time of flight–secondary ion mass spectrometry (TOF–SIMS) data were acquired using an ION TOF IV dual beam spectrometer. $Cs^{+}$ ions at 1 keV and 20 nA of ion fluency were used to sputter the films, rastering over an area of (150 $\times$ 150) $\mu m^2$. The analysis was performed in negative polarity using a $Ga^{+}$ primary ion beam, operating at 25 keV and 2 pA, and rastering over an area of (50 $\times$ 50) $\mu m^2$. Mass resolution $M/\Delta M$ was higher than 5000 and full spectra from 1 amu to 1000 amu were acquired during the depth profiles.

## 3. RESULTS

Figure 1 shows the GIXRD patterns of all as grown films. The curves for films *a* through *d* are almost equal (except that the sharper feature for film *d* is centred around $2\Theta = 28°$) and correspond to an amorphous structure, in agreement with findings by Aarik et al. [14]. Film *e*, instead, shows clear signs of crystallization, and peaks belonging to different reflections of the monoclinic phase [15] are present in the GIXRD patterns. Some peaks result as a convolution of the reflections from several families of planes (see Fig. 1), and are quite broad and not always very well defined. These characteristics suggest that a large amount of the amorphous phase is still present in the film. In particular, the large shoulder around the ($\bar{1}$ 1 1) reflection is related to the amorphous component, typical of films *a* through *d*. It is remarkable that $HfO_2$ films, grown in non-equilibrium conditions by ALD, crystallize in the monoclinic phase, exactly as expected from the phase diagram

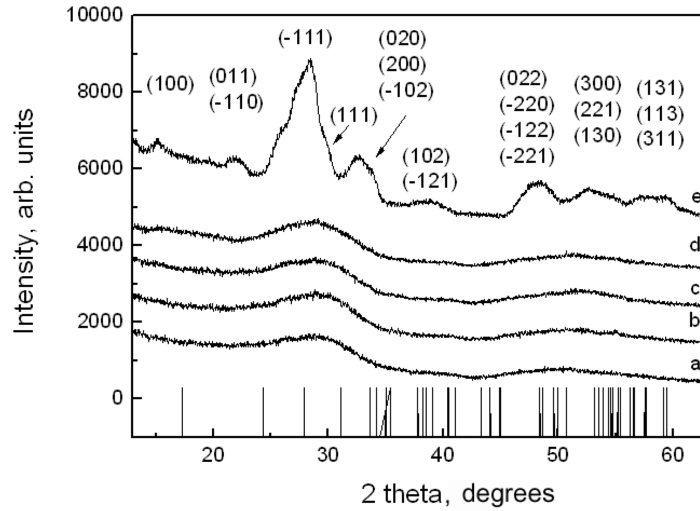


**Fig. 1.** GIXRD spectra of films *a* through *e*. The lines correspond to the peak positions as reported in [15].

([16,17] and references therein) at the pressure and temperature condition of the growth (Section 2).

Figure 2 shows the XRR spectra and the corresponding fitting for all films. The results of the fitting are presented in Tables 1 and 2. The following trends are observed: (i) the film thickness *d* decreases with increasing $T_g$; (ii) the growth rate $\gamma$ for films *a* through *e* decreases linearly up to $T_g$ = 300 °C, beyond which a plateau is reached; (iii) the electronic density $\delta$ increases with increasing $T_g$ and moves toward the bulk value (0.0599 Å$^{-3}$ for the monoclinic phase of $HfO_2$). This result is in agreement with Aarik et al. [14] and is clearly observed from the change of the critical angle (Fig. 3). Very likely films grown at lower $T_g$ are richer in impurities and porosity (reason for their lower density [18]); (iv) surface roughness $\sigma$ of the $HfO_2$ film measured from XRR shows no remarkable trend.

**Table 2.** Thickness ($d_{organic}$ and $d_{SiO_2}$) and roughness ($\sigma_{organic}$ and $\sigma_{SiO_2}$) of the organic material layer on top of the $HfO_2$ films and of the $SiO_2$ interfacial layer from the XRR analysis. The reported values are those providing the best fittings. The fourth column reports the roughness of the top layer surface measured with atomic force microscopy ($\sigma_{AFM}$)

| Film | $d_{organic}$, nm | $\sigma_{organic}$, nm | $\sigma_{AFM}$, nm | $d_{SiO_2}$, nm | $\sigma_{SiO_2}$, nm |
|---|---|---|---|---|---|
| *a* | – | – | 0.11 | 1.3 | 0.4 |
| *b* | 0.4 | 0.2 | 0.13 | 1.2 | 0.7 |
| *c* | 0.5 | 0.3 | 0.16 | 1.5 | 0.4 |
| *d* | 2.0 | 0.4 | 0.42 | 1.3 | 0.4 |
| *e* | 2.0 | 0.5 | 0.60 | 1.3 | 0.4 |

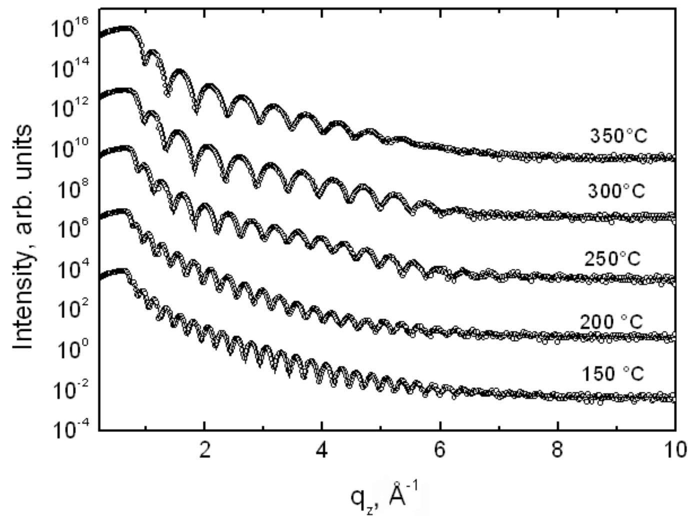


**Fig. 2.** XRR data and corresponding fitting for films *a* through *e*. $q_z$ in Figs. 2 and 3 is the perpendicular component of the scattering vector that, for a specular reflectivity experiment, is equal to $q_z = (4\pi/\lambda)sin(\Theta)$, where $\Theta$ is the angle of incidence.

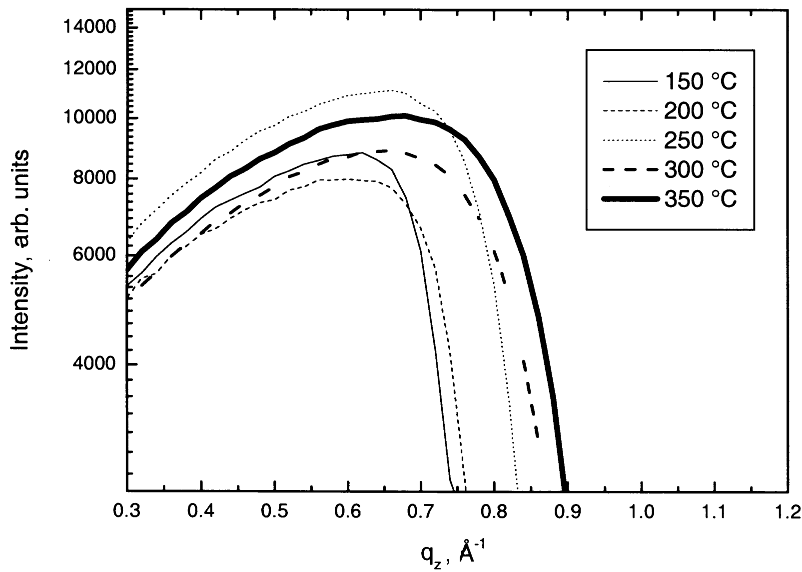


**Fig. 3.** Detail of the XRR spectra showing the change in the critical angle for films *a* through *e*. The trend is linked to modifications in the electronic density $\delta$.

The best fittings of the XRR data were obtained by adding a layer of organic material on top of the films (Table 2). No influence of this layer on the simulation of the XRR spectrum of film *a* was found. The layer of organic material is very thin and badly defined (roughness almost as high as film thickness) in films *b* and *c*. Finally, it reaches a stable value of thickness (higher than the roughness) in films *c* through *e*. Thickness and roughness of the $SiO_2$ interfacial layer are almost constant and close to the expected values for the native silicon oxide.

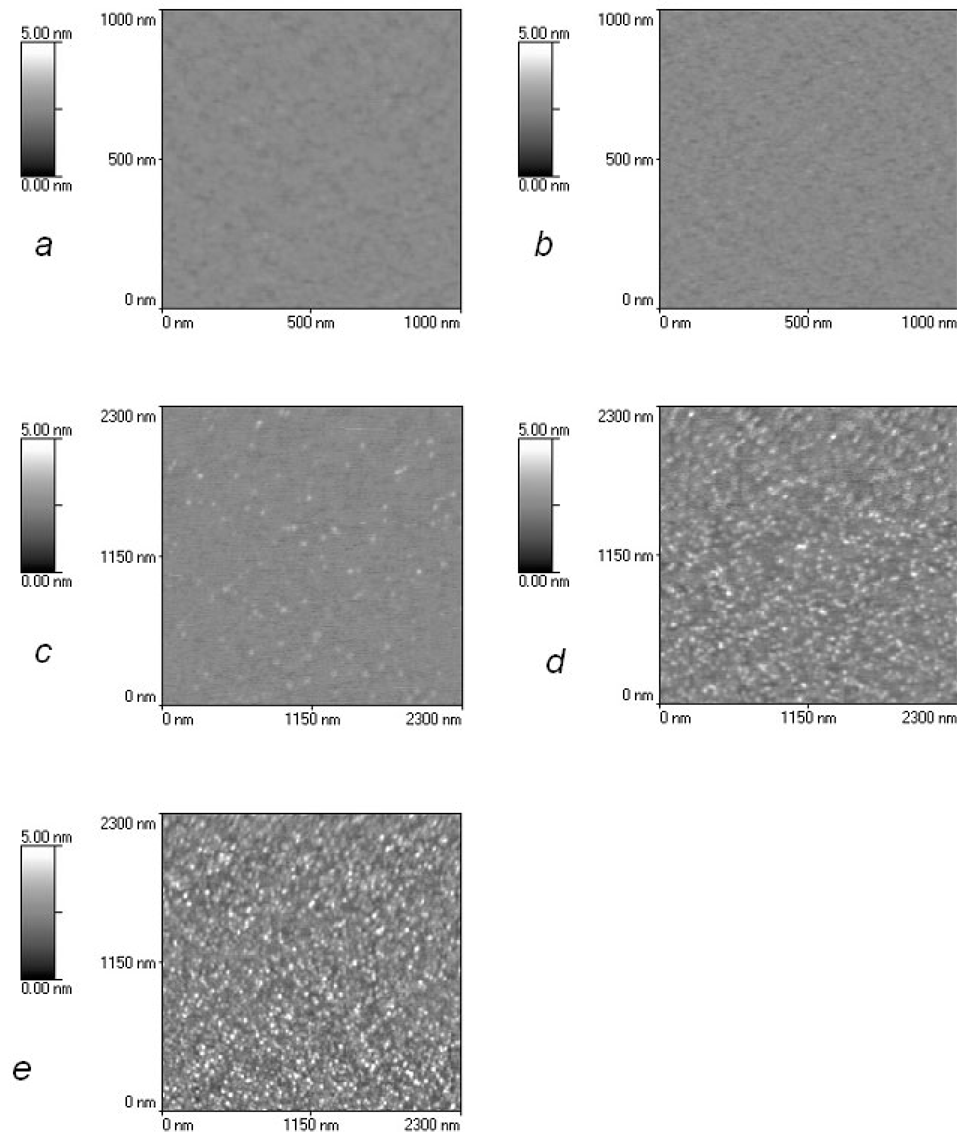


**Fig. 4.** AFM images of films *a* through *e*. The images are square scans of either 1 $\mu$m (films *a* and *b*) or 2.3 $\mu$m (films *c* through *e*) side, with a resolution of 300 points $\times$ 300 lines.

Atomic force microscopy images (Fig. 4) show a significant modification of the surface morphology with $T_{\mathrm{g}}$. In films *a* and *b*, the surface is flat, without particular features. Small structures ($\approx$ 20–40 nm wide and $\approx$ 1–2 nm high) start to emerge on the surface in films *c* through *e* and their density increases considerably with $T_{\mathrm{g}}$. Accordingly, the surface roughness values measured by AFM (Table 2) increase with $T_{\mathrm{g}}$. This trend is in agreement with the one found by XRR for the top layer roughness. The discrepancy in the AFM and XRR measured values is within the experimental errors ($\pm$ 0.1 nm for XRR and 10% for AFM).

A representative TOF–SIMS depth profile is shown in Fig. 5. Since acquisition was performed using $Cs^+$ in negative polarity, silicon and hafnium profiles were determined using $SiO_2$ and $^{180}HfO_2$ cluster signals. The $^{180}HfO_2$ profile is relatively flat throughout the film. The rise of the $SiO_2$ signal, not the $^{180}HfO_2$ intensity drop, marks the interface between $HfO_2$ and the interfacial $SiO_2$. Indeed, $^{180}HfO_2$ and $SiO_2$ signals drop at the same depth. This phenomenon is rather an artefact of the measurement than an indication that Hf contaminates the interfacial $SiO_2$.

Figure 6 reports chlorine depth profiles of films *a* through *e*. Chlorine concentration decreases with increasing $T_{\mathrm{g}}$. No calibration was done to obtain precise quantitative data on chlorine concentration. Nevertheless, given that we can reasonably assume the ion yield of chlorine to be the same as the one of oxygen [11] and that, considering the corresponding natural isotopic abundances, the signal of $^{18}O$ is 1% of the signal of $^{37}Cl$ in film *a* (data not shown), we can conclude that chlorine

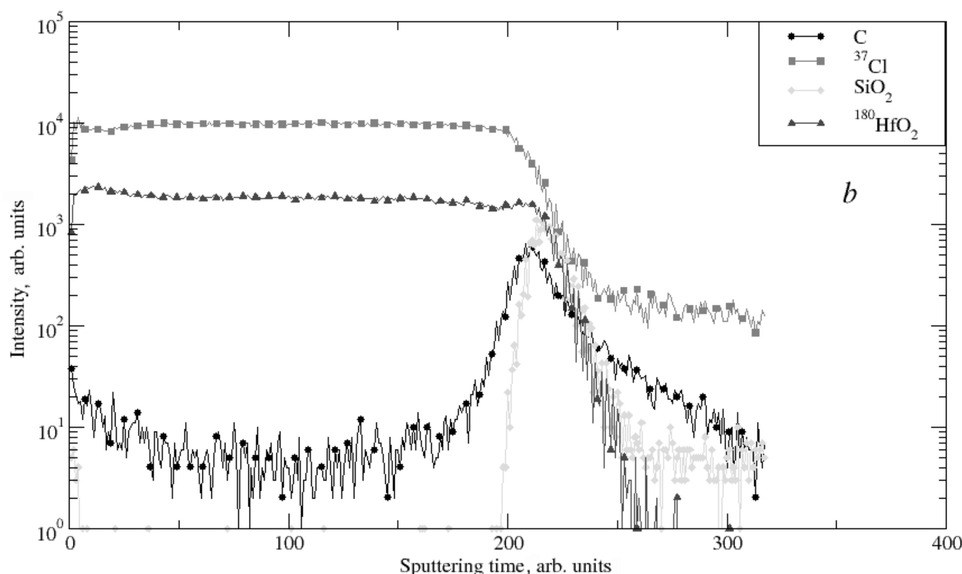


**Fig. 5.** TOF–SIMS profile of film *b*, representative of a typical depth profile on the set of films presented in this work.

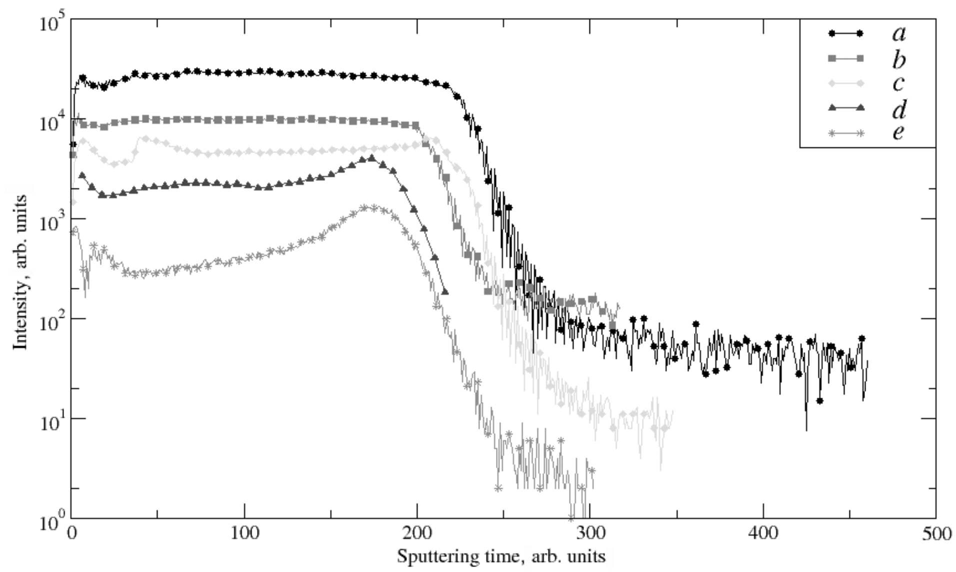


**Fig. 6.** Chlorine TOF–SIMS depth profiles of films *a* through *e*.

concentration in film *a* is as high as 50% of the amount of oxygen in the film, and it decreases to less than 1% in film *e*.

Figure 7 shows the TOF–SIMS profile of carbon in films *a* through *e*. All the films show a remarkable amount of carbon at the $HfO_2/SiO_2$ interface. We argue

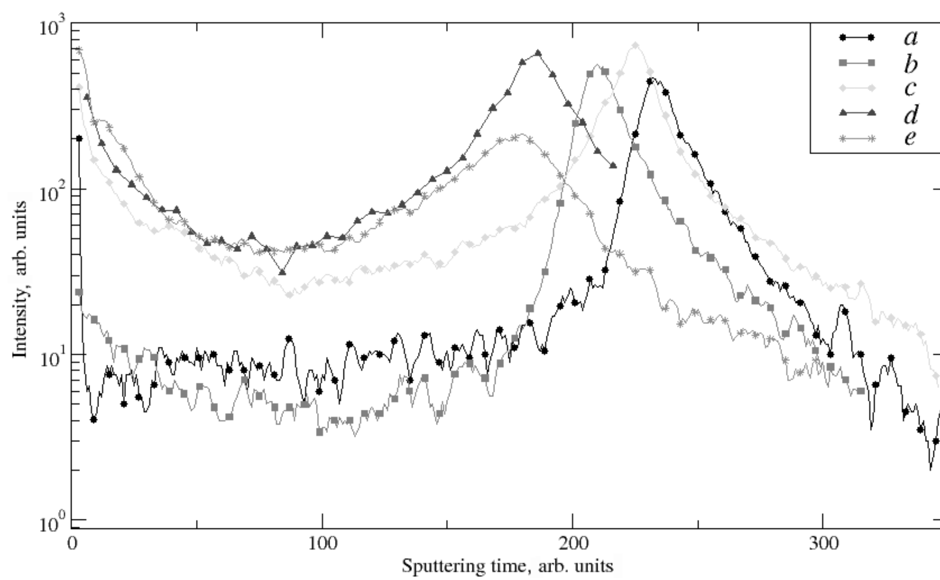


**Fig. 7.** Carbon TOF–SIMS depth profiles of films *a* through *e*.

that carbon contamination at the interface occurs before the start of the deposition process. The amount of carbon trapped at the interface does not depend on $T_g$ except in film *e*, in which the interfacial carbon peak is lower than in the other films. Carbon contamination in the film and at the surface, on the other hand, becomes apparent at $T_g > 250$ °C and increases very slightly with $T_g$. The temperature 250 °C is critical, above which the organic contaminants present in the growth chamber become reactive and are incorporated into the film. At the end of the deposition, in the films grown at $T_g > 250$ °C, more carbon can adsorb on the hot surface just before the start of the cooling process. This result is in agreement with XRR and AFM data, which detect, respectively, a well-defined layer of organic material on top of the films (Table 2) and wide superficial features of not well-defined nature (Fig. 4) for $T_g \geq 250$ °C.

## 4. DISCUSSION

### 4.1. Effects of the growth temperature on thin film growth

Three major bonds might be present on the silicon surface. According to Kim et al. [9], these are Si–(OH), Si–2(OH), and Si–O–Si bridging structures. The amount of these bonds is temperature dependent [14]. In particular, more $Si^{+1}$–$(OH)^{-1}$ bonds cover the silicon surface at lower temperatures (below 300 °C [19]) and transform into Si–O–Si bridging structures as temperature increases [20]. Note that at elevated temperatures O is most stably bonded when it forms Si–O–Si bridges [20]. As $ZrO_2$ films are grown by ALD from a chloride-based precursor ([10] and S. Haukka et al., unpublished results), we expect also $HfO_2$ films from $HfCl_4$ to develop two types of structures: an amorphous and a crystalline one. The former nucleates on Si–(OH) bonds and the latter when two Si–(OH) bonds react with one $HfCl_4$ molecule (*agglomeration reaction*; S. Haukka et al., unpublished results). Given the temperature dependent bond distribution mentioned before and activation energy for the agglomeration reaction, we expect a more amorphous $HfO_2$ film while growing at lower $T_g$. Our data (e.g. Fig. 1) and previous work by Aarik et al. [14] show that this is indeed the case. In [14], the authors underline that also the high chlorine content contributes to promoting the amorphous phase in the $HfO_2$ films grown at lower $T_g$.

### 4.2. Effects of the growth temperature on thin film composition

The growth temperature influences the reactions occurring during the ALD process which, in turn, affects the amount and the type of foreign species in the films. Our data indicate that chlorine and carbon are the dominating ones among these foreign species.

The presence of chlorine, similarly to the case of $ZrO_2$, may result in the formation of $Hf(OH)_2Cl_2$ (S. Haukka et al., unpublished results) or other similar

complexes [21]. These complexes are stable at lower values of $T_g$ (e.g., according to S. Haukka (private communication), $Hf(OH)_2Cl_2$ is stable only up to 150 °C) and decompose only for higher values of $T_g$. This fact explains why the amount of chlorine decreases as $T_g$ increases. The amount of residual chlorine remaining in $HfO_2$ and $ZrO_2$ films grown in similar conditions is approximately the same in both films as shown elsewhere [10,11]. Finally, the higher concentration of chlorine in films *a* and *b* is well correlated also with the lower density of these two films compared to the others and to the value expected for bulk $HfO_2$.

### 4.3. Different behaviour of $HfO_2$ and $ZrO_2$ in non-equilibrium growth conditions

Studies of the crystalline structures of $HfO_2$ and $ZrO_2$ ([16,17,22] and references therein), underline the structural similarity of $HfO_2$ and $ZrO_2$ and claim that the two materials should always exhibit similar properties. However, comparing the results of this work with those for $ZrO_2$ films grown in similar conditions [10], we show that $HfO_2$ and $ZrO_2$ thin films grown in non-equilibrium conditions using ALD behave differently. Indeed, our data show that $HfO_2$ films remain amorphous up to higher growth temperatures than $ZrO_2$ films, and become crystalline only at a growth temperature above 300 °C, whereas $ZrO_2$ films become crystalline already at 250 °C [10]. From this observation we might infer that the crystalline $HfO_2$ component starts crystallization at higher growth temperatures than the $ZrO_2$ films [10]. In addition, our measurements show that compared to $ZrO_2$ the growth-time crystallization of $HfO_2$ begins at a higher thickness. Moreover, $HfO_2$ crystallizes in the monoclinic phase, as expected from the phase diagram at ambient temperature and pressure ([16,17,22] and references therein), whereas $ZrO_2$ develops in the tetragonal phase before transforming into the monoclinic phase [10,23,24], the one predicted by the phase diagram. Finally, for lower growth temperatures, the growth rate $\gamma$ is higher for $HfO_2$ than for $ZrO_2$ [10] grown in the same conditions and the film density $\delta$ is anomalously low for $HfO_2$ (Table 1).

It is very difficult to explain the above listed differences between $HfO_2$ and $ZrO_2$ [10] films grown by ALD using chlorine-based precursors. The films we compare using our results and those of [10] were grown on the same type of Si(1 0 0) substrate with native oxide, using the same precursor purge and pulse times, and finally, the same precursor source temperature. Since also the same growth temperature sequence was followed, the same distribution of reactive sites was present on the initial surface during the growth of the $HfO_2$ and $ZrO_2$ films. Therefore, having ruled out an argument based on reactive sites on the inital surface, something related to the film nature must cause non-equivalent responses of the two oxides. However, neither the ionic character, very similar for $HfO_2$ and $ZrO_2$ (we calculated the ionicity of $HfO_2$ and $ZrO_2$ [25] to be respectively 70% and 67%) nor the ionic radius of the metals, very similar too (0.078 nm for $Hf^{+4}$ and 0.079 nm for $Zr^{+4}$ [16]) for the free atoms in an inert atmosphere, are sufficient

to explain the differences. Perhaps, these reside in the nature of the crystalline component of the $HfO_2$ and $ZrO_2$ films, given that most of them are related with the way crystallization occurs. We suggest the following hypotheses: (i) a different thermodynamics of grain nucleation and growth of the crystalline component in $HfO_2$ and $ZrO_2$ films, or (ii) a different response to impurities (such as $Cl^-$ ions, which behave differently in the two oxide films but are less than 1% of the oxygen content in both $HfO_2$ and $ZrO_2$ films grown at $T_g$ = 350 °C. Note that this value of $T_g$ gives rise, for both oxides, to the more markedly crystalline films [[26]]. It has been shown that compared to $ZrO_2$ the temperature at which $HfO_2$ still grows amorphous is higher [[10]]. The authors of [[26]] attributed this effect to the presence of Si in $HfO_2$ films. We cannot rely on this explanation, as our films, with the exception of their surface and interface, do not contain Si. Further investigation is needed to clarify this point.

## 5. CONCLUSIONS

$HfO_2$ films were grown by atomic layer deposition, varying the growth temperature $T_g$ in the range between 150 °C and 350 °C. It was found that $T_g$ affected the structural and compositional characteristics of the films, and also the growth rate. In particular, increasing $T_g$ promoted the formation of crystallites in the monoclinic phase and a decrease in the chlorine concentration. Moreover, at higher $T_g$, the carbon contained in the contaminants present in the growth chamber became more reactive toward the film surface. Finally, $HfO_2$ films were found to grow amorphous up to higher values of $T_g$ than $ZrO_2$ films grown in similar conditions. Our results show that $T_g$ indeed plays a role in tuning the structural and compositional characteristics of $HfO_2$ films grown by atomic layer deposition.

## ACKNOWLEDGEMENT

This work was partially supported by the European Project ESQUI (Project No. GRD 1-999-11097).

## REFERENCES

1. Wilk, G. D., Wallace, R. M. and Anthony, J. M. High-$k$ gate dielectrics: current status and materials properties considerations. *J. Appl. Phys.*, 2001, **89**, 5243–5275.
2. Kingon, A. I., Maria, J.-P. and Streiffer, S. K. Alternative dielectrics to silicon dioxide for memory and logic devices. *Nature*, 2000, **406**, 1032–1038.
3. Robertson, J. Schottky barrier heights in wide gap oxides and implications for future electronic devices. *J. Vac. Sci. Technol. B*, 2000, **18**, 1785–1791.
4. Robertson, J. Electronic structure and band offsets of high-dielectric-constant gate oxides. *MRS Bulletin*, 2002, **27**, 217–221.
5. Hubbard, K. J. and Schlom, D. G. Thermodynamic stability of binary oxides in contact with silicon. *J. Mater. Res.*, 1996, **11**, 2757–2776.

6. Schlom, D. G. and Haeni, J. H. A thermodynamic approach to selecting alternative gate dielectrics. *MRS Bulletin*, 2002, **27**, 198–205.
7. Ritala, M., Kukli, K., Rahtu, A., Räisänen, P. I., Leskelä, M., Sajavaara, T. and Keinonen, J. Atomic layer deposition of oxide thin films with metal alkoxides as oxygen sources. *Science*, 2000, **288**, 319–321.
8. Cosnier, V., Olivier, M., Théret, G. and André, B. $HfO_2$–$SiO_2$ interface in PVD coatings. *J. Vac. Sci. Technol. A*, 2001, **19**, 2267–2271.
9. Kim, Y. B., Tuominen, M., Raaijmakers, I., de Blank, R., Wilhelm, R. and Haukka, S. Initial stage of the ultrathin oxide growth in water vapor on Si(100) surface. *Electrochem. Solid-State Lett.*, 2000, **3**, 346–349.
10. Scarel, G., Ferrari, S., Spiga, S., Tallarida, G., Wiemer, C. and Fanciulli, M. Effect of growth temperature on the properties of atomic layer deposition grown $ZrO_2$ films. *J. Vac. Sci. Technol. A*, 2003, **21** (in press).
11. Ferrari, S., Scarel, G., Wiemer, C. and Fanciulli, M. Chlorine mobility during annealing in $N_2$ in $ZrO_2$ and $HfO_2$ films grown by atomic layer deposition. *J. Appl. Phys.*, 2002, **92**, 7675–7677.
12. Kukli, K., Ritala, M., Aarik, J., Uustare, T. and Leskelä, M. Influence of growth temperature on properties of zirconium dioxide films grown by atomic layer deposition. *J. Appl. Phys.*, 2002, **92**, 1833–1840.
13. Cho, M., Park, J., Park, H. B., Hwang, C. S., Jeong, J. and Hyun, K. S. Chemical interaction between atomic-layer-deposited $HfO_2$ thin films and the Si substrate. *Appl. Phys. Lett.*, 2002, **81**, 334–336.
14. Aarik, J., Aidla, A., Kiisler, A.-A., Uustare, T. and Sammelselg, V. Influence of substrate temperature on atomic layer growth and properties of $HfO_2$ thin films. *Thin Solid Films*, 1999, **340**, 110–116.
15. Inorganic Crystal Structure Database. File 27313 for monoclinic $HfO_2$. Fachinformazionzentrum Karlsruhe, 2002.
16. Zhao, X. and Vanderbilt, D. First-principles study of structural, vibrational, and lattice dielectric properties of hafnium oxide. *Phys. Rev. B*, 2002, **65**, 233106.
17. Desgreniers, S. and Lagarec, K. High-density $ZrO_2$ and $HfO_2$: crystalline structures and equations of state. *Phys. Rev. B*, 1999, **59**, 8467–8472.
18. Kukli, K., Ritala, M., Uustare, T., Aarik, J., Forsgren, K., Sajavaara, T., Leskelä, M. and Hårsta, A. Influence of thickness and growth temperature on the properties of zirconium oxide films grown by atomic layer deposition on silicon. *Thin Solid Films*, 2002, **410**, 53–60.
19. Haukka, S., Lakomaa, E.-L. and Suntola, T. Adsorption controlled preparation of heterogeneous catalysts. In *Adsorption and Its Applications in Industry and Environmental Protection* (Dabrowski, A., ed.). Elsevier, Amsterdam, 1998, 715–750.
20. Green, M. L., Gusev, E. P., Degraeve, R. and Garfunkel, E. L. Ultrathin ($<4$ nm) $SiO_2$ and Si–O–N gate dielectric layers for silicon microelectronics: understanding the processing, structure, and physical and electrical limits. *J. Appl. Phys.*, 2001, **90**, 2057–2121.
21. Widjaja, Y. and Musgrave, C. B. Quantum chemical study of the elementary reactions in zirconium oxide atomic layer deposition. *Appl. Phys. Lett.*, 2002, **81**, 304–306.
22. Zhao, X. and Vanderbilt, D. Phonons and lattice dielectric properties of zirconia. *Phys. Rev. B*, 2002, **65**, 075105.
23. Evangelou, E. K., Scarel, G., Ferrari, S., Spiga, S., Tallarida, G., Wiemer, C., Dekadjevi, D. T., Fanciulli, M. and Pavia, G. Thickness dependent properties and stability of ALD grown zirconium dioxide films. *J. Appl. Phys.* (submitted).
24. Bonera, E., Scarel, G. and Fanciulli, M. Structure evolution of atomic layer deposition grown $ZrO_2$ films by deep-ultra-violet Raman and far-infrared spectroscopies. *J. Non-Cryst. Solids*, 2003, **322**, 105–110.

25. Callister, W. D. *Materials Science and Engineering: an Introduction*. Wiley, New York, 1997.
26. Neumayer, D. A. and Cartier, E. Materials characterization of $ZrO_2$–$SiO_2$ and $HfO_2$–$SiO_2$ binary oxides deposited by chemical solution deposition. *J. Appl. Phys.*, 2001, **90**, 1801–1808.

# Kasvutemperatuuri mõju $HfO_2$ aatomkihtsadestatud kilede omadustele

Giovanna Scarel, Claudia Wiemer, Sandro Ferrari, Grazia Tallarida ja Marco Fanciulli

Hafniumdioksiidi elektrilised ja soojuslikud omadused teevad ta üheks perspektiivseimaks ränidioksiidi asendajaks metalloksiid-pooljuhtstruktuurides. On uuritud aatomkihtsadestuse abil kasvatatud $HfO_2$ kilede struktuurseid omadusi ja koostist kasvutemperatuuride vahemikus 150–350 °C, kasutades selleks röntgendifraktsiooni ja -peegelduse, aatomjõumikroskoopia ning sekundaarioonide massispektromeetria meetodit. Kõrgem kasvutemperatuur soodustab kristalliitide teket monokliinses faasis ja kilede saastumist süsinikuga kasvukambris. Võrreldes $ZrO_2$ kiledega jäävad $HfO_2$ kiled amorfseteks kõrgete kasvutemperatuurideni.